

Key Points:

- The whistler-mode waves with power gaps around $0.5\Omega_e$ in the Earth's magnetosphere are investigated by 2-D PIC simulations
- The power gap is formed due to the severe damping by the plateau-like electron component in the parallel velocity distribution at $\sim 0.5V_{Ae}$
- The plateau-like distribution in the parallel direction is caused by the nonparallel wave modes through Landau resonance

Supporting Information:

Supporting Information may be found in the online version of this article.

Correspondence to:

X. Gao and Q. Lu,
gaoxl@mail.usc.edu.cn;
qmlu@usc.edu.cn






Citation:

Chen, H., Gao, X., Lu, Q., Fan, K., Ke, Y., Wang, X., & Wang, S. (2022). Gap formation around $0.5\Omega_e$ in the whistler-mode waves due to the plateau-like shape in the parallel electron distribution: 2D PIC simulations. *Journal of Geophysical Research: Space Physics*, 127, e2021JA030119. <https://doi.org/10.1029/2021JA030119>

Received 9 NOV 2021

Accepted 4 APR 2022

Gap Formation Around $0.5\Omega_e$ in the Whistler-Mode Waves Due To the Plateau-Like Shape in the Parallel Electron Distribution: 2D PIC Simulations

Huayue Chen^{1,2} , Xinliang Gao^{1,2} , Quanming Lu^{1,2} , Kai Fan^{1,2} , Yangguang Ke^{1,2}, Xueyi Wang³ , and Shui Wang^{1,2}

¹CAS Key Laboratory of Geoscience Environment, School of Earth and Space Sciences, University of Science and Technology of China, Hefei, China, ²CAS Center for Excellence in Comparative Planetology, Hefei, China, ³Department of Physics, Auburn University, Auburn, AL, USA

Abstract The power gap around $0.5\Omega_e$ (where Ω_e is the equatorial electron gyrofrequency) of whistler-mode waves is commonly observed in the Earth's inner magnetosphere, but its generation mechanism is still under debate. By performing two-dimensional particle-in-cell simulations in a uniform background magnetic field, we investigate the spectral properties of whistler-mode waves excited by temperature anisotropic electrons. The waves have positive growth rates in a wide range of normal angles ($\theta \approx 0^\circ\text{--}35^\circ$), resulting in the generation of both parallel and nonparallel waves. Although the nonparallel wave modes are weaker than the parallel ones, they can cause the plateau-like shape around $0.5 V_{Ae}$ (where V_{Ae} represent the electron Alfvén speed) in the parallel direction of electron velocity distribution. The plateau-like electron component can then lead to severe damping in the waves around $0.5\Omega_e$ via the cyclotron resonance, and the power gap is formed. This mechanism is called as “spectrum bite”. Our study sheds fresh light on the well-known gap formation at $\sim 0.5\Omega_e$ in the whistler-mode waves, which is ubiquitously detected near the equator in the inner magnetosphere.

1. Introduction

Whistler-mode waves are intense electromagnetic emissions ubiquitously observed in the Earth's inner magnetosphere (Burtis & Helliwell, 1969; L. J. Chen et al., 2013; Santolík et al., 2005; Tsurutani & Smith, 1974, 1977). They can not only efficiently scatter low-energy (0.1–30 keV) electrons into the loss cone and cause diffuse aurora in the upper atmosphere (Kasahara et al., 2018; Ni et al., 2008), but also accelerate seed electrons (~ 100 keV) to relativistic energies ($\sim \text{MeV}$), refilling the outer radiation belt during geoactive storms (Horne et al., 2003; Summers et al., 1998; Thorne et al., 2013). Besides the typical exhibition of the frequency chirping (Burtis & Helliwell, 1969; H. Chen et al., 2022; X. L. Gao et al., 2014; Ke et al., 2017, 2020; Lu et al., 2019; Omura et al., 2009; Tsurutani & Smith, 1974, 1977) and repetitive emissions (H. Chen et al., 2022; Hikishima et al., 2010; Lu et al., 2021; Tsurutani et al., 2013), another notable characteristic of whistler-mode waves in the Earth's magnetosphere is the power gap around $0.5\Omega_e$ (where Ω_e is the equatorial electron gyrofrequency), which visually separates the spectrum into a lower band (0.1– $0.5\Omega_e$) and an upper band ($0.5\text{--}0.8\Omega_e$) (Fu et al., 2014; X. Gao et al., 2019; W. Li et al., 2011; Tsurutani & Smith, 1974).

The power gap of whistler-mode waves in the inner magnetosphere was firstly discovered by Tsurutani and Smith (1974) over ~ 50 years ago, and the Landau damping is thought to play a critical role in the occurrence of such a gap. After that, several efforts have been made to uncover the generation mechanisms of the gap (H. Chen et al., 2021; H. Y. Chen et al., 2017; Fu et al., 2014, 2017; X. Gao et al., 2017; X. L. Gao et al., 2016; J. Li et al., 2019; Liu et al., 2011; Omura et al., 2009; Ratcliffe & Watt, 2017). Liu et al. (2011) and Fu et al. (2014) have suggested that lower-band and upper-band whistler-mode waves can be independently excited by two distinct electron populations, leaving a power gap between them. By performing one-dimensional (1-D) particle-in-cell (PIC) simulations of nonparallel whistler-mode waves excited by an anisotropic electron distribution, J. Li et al. (2019) have found that the electron distribution could be separated into two anisotropic populations due to Landau resonance, which then excite whistler-mode waves with two bands. However, the gap formation is sensitively dependent on particular choices of plasma parameters, and even fails in some circumstances by only extending to a two-dimensional (2-D) frame (Ratcliffe & Watt, 2017). Based on THEMIS satellites, X. L. Gao et al. (2016) have firstly reported the “multiband chorus” in the Earth's magnetosphere, which is explained by the nonlinear wave-wave coupling (i.e., lower band cascade). This mechanism has been supported by both

PIC simulations (H. Y. Chen et al., 2017; X. Gao et al., 2017) and observational results (X. Gao et al., 2018). While, a statistical analysis of the power gap (X. Gao et al., 2019) has implied that the lower band cascade is only able to explain part of banded whistler-mode chorus events. Omura et al. (2009) have proposed that, as whistler-mode waves propagate away from the magnetic equator, that is, source region, they will become nonparallel and experience severe nonlinear Landau damping at $0.5\Omega_e$. This effect is supposed to become significant after waves propagate far away from the source region. Nevertheless, satellite observations have illustrated that whistler-mode waves with banded structures are typically generated near the magnetic equator (X. Gao et al., 2019; Teng et al., 2019).

Recently, with a 1-D PIC model, H. Chen et al. (2021) have demonstrated that an electron velocity distribution with a plateau-like component at $\sim 0.5V_{Ae}$ (where V_{Ae} is the electron Alfvén speed) in the parallel direction, resulting from the Landau resonance of nonparallel whistler-mode waves, can cause severe damping around $0.5\Omega_e$, and then the spectrum of the waves naturally forms a gap at $\sim 0.5\Omega_e$. In their model, whistler-mode waves excited by anisotropic electrons are all fixed at a finite wave normal angle (WNA), whereas both linear theory (Fan et al., 2019; Gary et al., 2011) and multi-dimensional PIC simulations (Lu et al., 2019) have confirmed that the wave mode with the maximum growth rate propagates along the background magnetic field. Therefore, the proportion of plateau-like electrons will be artificially amplified in H. Chen et al. (2021). Whether this mechanism is still valid in a multi-dimensional (more realistic) frame remains unknown.

In this study, by extending to a 2-D PIC model, we explore the gap formation in the whistler-mode waves excited by anisotropic electron distributions, and the wave modes exhibit a wide range of WNAs. Although the wave mode with the maximum growth rate propagates along the background magnetic field, a minor nonparallel component can produce a plateau-like component in electron distribution. The gap at $\sim 0.5\Omega_e$ is eventually formed in the power spectra for both nonparallel and strictly parallel whistler-mode waves.

2. Simulation Model and Initial Setup

We have employed a 2-D PIC simulation model with periodic boundary conditions to investigate the evolution of whistler-mode waves excited by the temperature anisotropic electrons. This model only allows spatial variations in the x and y directions, but it includes three components of electromagnetic fields and particle velocities. The electric and magnetic fields are updated by the Maxwell equations with an explicit “Leapfrog” algorithm, and the motions of particles are governed by the Lorentz equation. The electrons consist of cold and warm components (denoted by the subscripts “c” and “w”, respectively.), while the protons are treated as fixed background by assuming the mass ratio between proton and electron to be infinite.

The background magnetic field B_0 is assumed to be uniform, which is along the x axis. The ratio between plasma frequency and cyclotron frequency is set as $\omega_{pe}/\Omega_e = 4.0$. The cold electrons satisfy the Maxwellian distribution, with the plasma beta of $\beta_c = 2\mu_0 n_0 k_B T_c / B_0^2 = 10^{-4}$ and the number density of $n_c = 0.85n_0$. While the warm electrons satisfy the bi-Maxwellian distribution with the temperature anisotropy of $T_{\perp w}/T_{\parallel w} = 4.0$. Their parallel plasma beta and number density are assumed to be $\beta_{\parallel w} = 2\mu_0 n_0 k_B T_{\parallel w} / B_0^2 = 0.09$ and $n_w = 0.15n_0$. The temperature of protons is same as that of cold electrons. These initial parameters are all typical values at L -shell = 6. The simulation domain has 1,024 grid cells in the x direction with the grid size of $\Delta x = 0.6\lambda_e$ (where $\lambda_e = c/\omega_{pe}$ is the electron inertial length, c is the light speed), and 256 cells in the y direction with $\Delta y = 0.6\lambda_e$. We uniformly set 6,000 macroparticles for each species in each cell, and the time step in our simulation is $0.025\Omega_e^{-1}$.

3. Simulation Results

Figure 1 illustrates the time history of temperature anisotropy of warm electrons $T_{\perp w}/T_{\parallel w}$ and fluctuating magnetic field strength $\delta B/B_0$ ($\delta B = \sqrt{\delta B_x^2 + \delta B_y^2 + \delta B_z^2}$), which are represented by blue and red lines, respectively. The temperature anisotropy starts to decrease from $\sim 100\Omega_e^{-1}$, resulting in the excitation of whistler-mode waves. The waves grow exponentially till $\sim 240\Omega_e^{-1}$ and saturate at $\sim 328\Omega_e^{-1}$, with the maximum amplitude reaching up to $\delta B/B_0 \approx 0.024$. The amplitude then decreases rapidly. To further investigate the wave spectrum, the linear growth rates have been calculated by the PDRK model (Xie & Xiao, 2016) with the initial setup. Figure 2a shows the growth rate γ as a function of (k_x, k_y) , with the dotted lines representing wave frequency contour lines. The waves

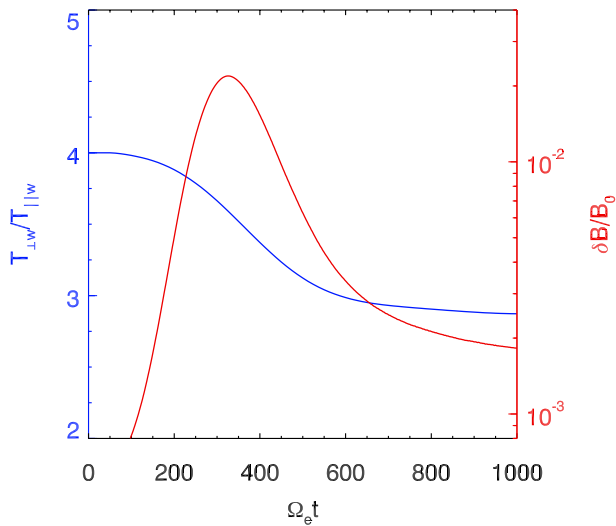


Figure 1. The temporal history of temperature anisotropy of warm electrons $T_{\perp w}/T_{\parallel w}$ and fluctuating magnetic field strength $\delta B/B_0$, which are represented by blue and red lines.

have positive growth rates in a wide range of WNAs ($\theta \approx 0^\circ\text{--}35^\circ$), and the dominant mode (the wave mode with largest growth rate, denoted by the white asterisk) is located at $k_x \lambda_e = 1.28$ and $k_y \lambda_e = 0.0$, whose frequency is $\omega_d/\Omega_e = 0.57$. The spectra of magnetic fluctuation $\delta B/B_0$ in the k_x - k_y plane at $\Omega_e t =$ (b) 140, (c) 328, (d) 472, (e) 512, and (f) 658 have also been shown in Figure 2, where the wave numbers corresponding to the frequency of $0.5\Omega_e$ are represented by the black dotted line in each panel. The waves with frequencies greater than $0.5\Omega_e$ firstly generate at $\sim 140\Omega_e^{-1}$ (Figure 2b), and the wave mode with peak amplitude is found at $k_x \lambda_e = 1.26$ and $k_y \lambda_e = 0.0$ (represented by the red asterisk). This is consistent with the most unstable mode predicted by the linear theory, implying the whistler-mode waves are excited by the anisotropic electrons. When the waves saturate at $\sim 328\Omega_e^{-1}$ (Figure 2c), the spectrum exhibits a continuous band across $0.5\Omega_e$, and both parallel and nonparallel waves are excited. As time increases, the amplitudes of nonparallel waves around $0.5\Omega_e$ decrease significantly, and the power gap is formed, marked by the red frame in Figure 2d. Subsequently, the strictly parallel waves around $0.5\Omega_e$ are also damped, leading to the pronounced power gap in both parallel and nonparallel waves (Figures 2e and 2f). As shown in Movie S1, the power gap persists till the end of the simulation.

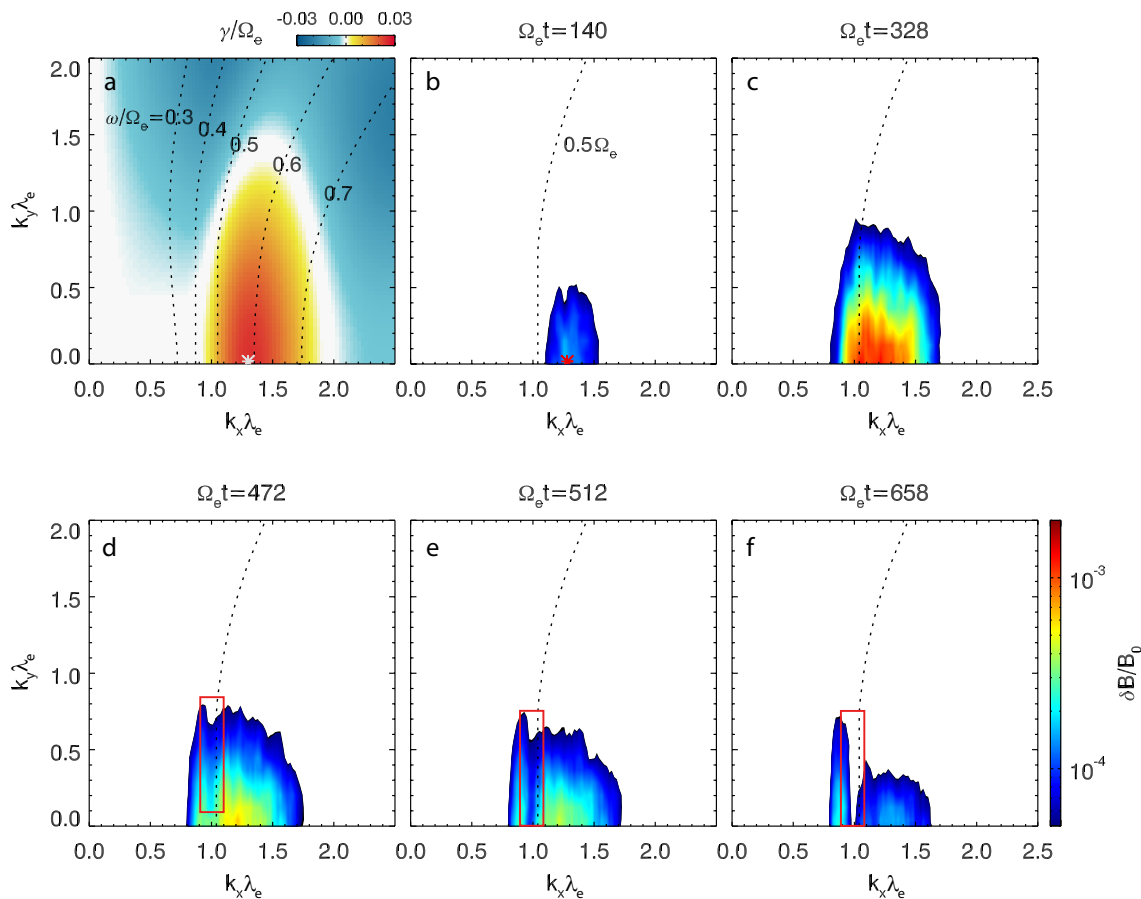


Figure 2. (a) The linear growth rate γ/Ω_e calculated with the initial setup, in which the black dotted lines denote the contour lines of wave frequencies and the white asterisk marks the wave mode with the largest growth rate. The spectrum of fluctuating magnetic fields $\delta B/B_0$ in the k_x - k_y plane at $\Omega_e t =$ (b) 140, (c) 328, (d) 472, (e) 512, and (f) 658. In the panels (b–f), the black dotted lines denote the wave numbers correspond to $\omega/\Omega_e = 0.5$, and the red asterisk in panel (b) represents the wave mode with the peak amplitude. The red rectangles in the panels (d–f) mark the power gaps in the wave spectrum.

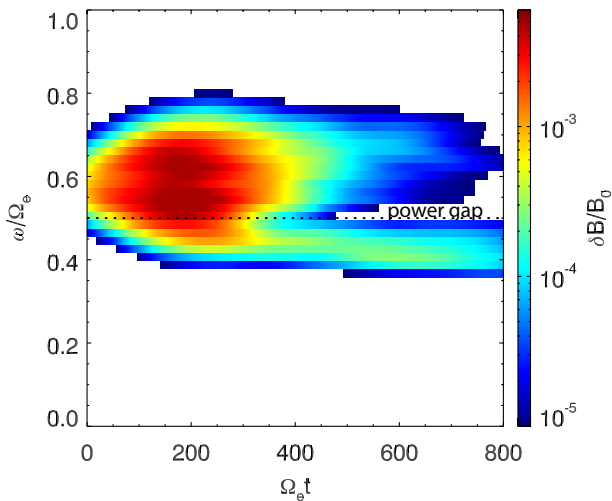


Figure 3. The ω - t spectrogram of $\delta B/B_0$, where the black dotted line denotes the frequency of $0.5\Omega_e$.

The ω - t spectrogram of the excited waves has been further investigated. Here we extract the magnetic field data from 16 points, which are uniformly distributed in the simulation domain. At each point, we perform the sliding short-time Fourier analysis to the magnetic fields with a window of $200\Omega_e^{-1}$. Then an average is conducted over these 16 points. The ω - t spectrogram of $\delta B/B_0$ is shown in Figure 3, where the black dashed line denotes $\omega = 0.5\Omega_e$. The waves with frequencies greater than $0.5\Omega_e$ are firstly excited. As the electron temperature anisotropy decreases, the frequency of the dominant wave mode also decreases, leading to the generation of visible wave power around and even below $0.5\Omega_e$. However, the waves around $0.5\Omega_e$ are severely damped after $\sim 300\Omega_e^{-1}$, and a gap is consequently formed. The power gap can split the spectrum into two frequency bands, which is quite similar to the banded structure in the whistler-mode waves observed in the Earth's magnetosphere.

Whistler-mode waves can play an important role in regulating electron velocity distribution. Figure 4a displays the parallel velocity distribution of warm electrons at $\Omega_e t = 500$ (black line), where the distribution at $\Omega_e t = 0$ (gray line) is overplotted for reference. Remarkably, two symmetric plateau-like shapes are formed around $\pm 0.5V_{Ae}$, denoted by two arrows. Based on the dispersion relation of whistler-mode waves, the Landau resonance velocities are close to $0.5V_{Ae}$ (further shown in Figure 8), so the plateau-like shape is produced here. The proportion of plateau-like distribution electrons can be

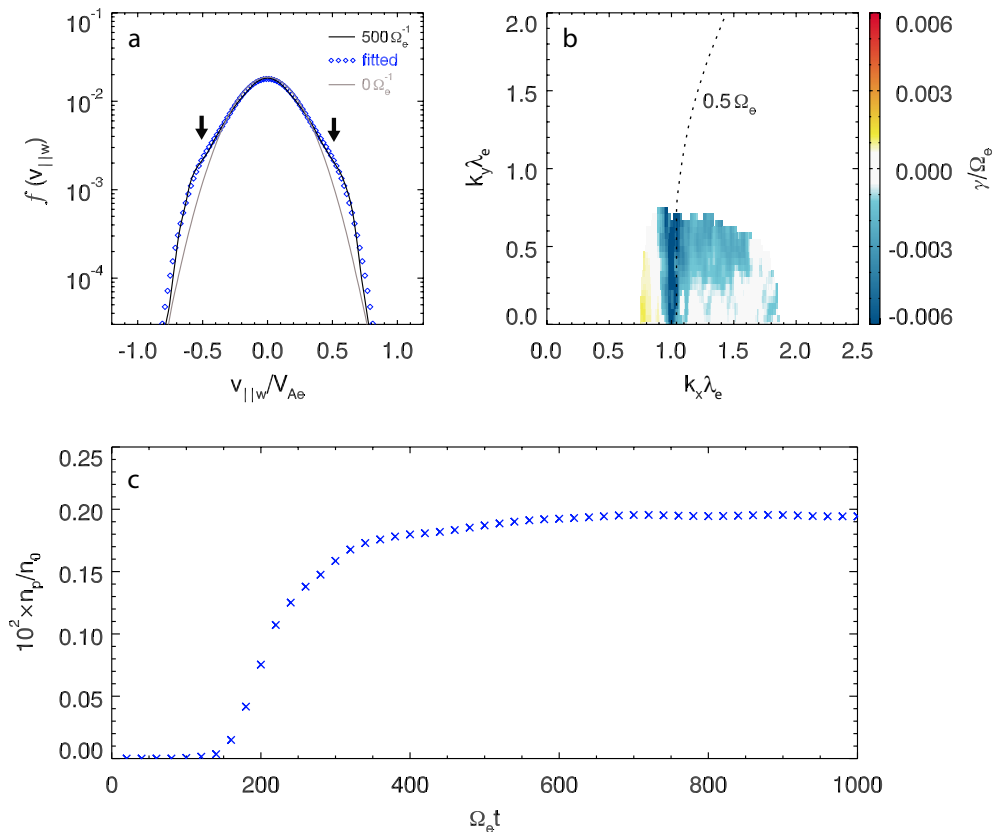


Figure 4. (a) The parallel velocity distributions of warm electrons at $500\Omega_e^{-1}$ (black line) and at $0\Omega_e^{-1}$ (gray line), and the blue diamonds represent the fitted curve at $500\Omega_e^{-1}$. Two symmetric plateau-like shapes are denoted by the black arrows. (b) The growth rate as a function of (k_x, k_y) around $500\Omega_e^{-1}$, in which the dotted line denotes the wave numbers corresponding to $0.5\Omega_e$. (c) The temporal evolution of n_p/n_0 , which is estimated following the method in panel (a).

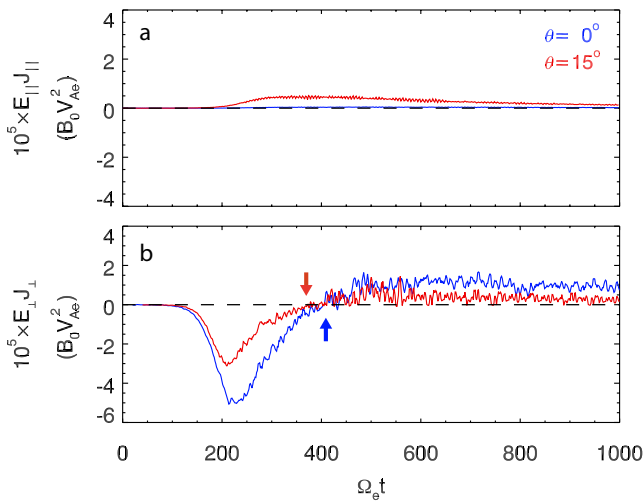


Figure 5. The temporal evolution of (a) $E_{\parallel} J_{\parallel}$ and (b) $E_{\perp} J_{\perp}$ around $0.5\Omega_e$, where the wave modes with $\theta = 0^\circ$ and $\theta = 15^\circ$ are denoted by the blue and red lines, respectively. In panel (b), the blue (red) arrow marks the time point when the wave mode with $\theta = 0^\circ$ ($\theta = 15^\circ$) starts to damp.

estimated by fitting the parallel velocity function with a combination of three Maxwellian distributions $f = \sum_{i=1}^3 f_i$ (i.e., hot and two symmetric plateau-like components, denoted by “h” and “p”, respectively), where

$$f_i = \frac{n_i}{\pi^{1/2} v_{\parallel th,i}} \exp\left(-\frac{(v_{\parallel} - v_{b,i})^2}{v_{\parallel th,i}^2}\right)$$

here, v_{\parallel} is the parallel velocity, and n_i , $v_{\parallel th,i}$, and $v_{b,i}$ are the number density, parallel thermal velocity, and bulk velocity of the i component. The distribution function is fitted by using the least square method, and the fitting curve is represented by the blue diamonds in Figure 4a. For the hot electron component, the number density is $n_h/n_0 = 14.64\%$ and thermal velocity is $v_{\parallel th,h}/V_{Ae} = 0.292$. While those of each plateau-like component are $n_p/n_0 = 0.18\%$ and $v_{\parallel th,p}/V_{Ae} = 0.165$, and their bulk velocities are $v_{b,p}/V_{Ae} = \pm 0.473$. To identify the influence of the plateau-like electron component on wave spectrum, we have then calculated the growth rate γ around $500\Omega_e^{-1}$, which is estimated by the time variation of the fluctuating magnetic field during the period of $\Omega_e t = 490\text{--}510$. Figure 4b displays the growth rate γ as a function of (k_x, k_y) , with the black dotted line representing the wave numbers corresponding to $0.5\Omega_e$. As the temperature anisotropy decreases, the wave modes with lower frequencies (or wave numbers) will be excited.

Therefore, the wave modes at $k_x \lambda_e = 0.8\text{--}0.9$ (corresponds to frequencies of $0.35\text{--}0.41\Omega_e$) have weakly positive growth rates. While other wave modes decay after $\sim 500\Omega_e^{-1}$, especially for the nonparallel waves. Remarkably, the wave modes around $0.5\Omega_e$ are more severely damped than those at other frequencies, due to the existence of plateau-like electron component. The peak proportion of the plateau-like component has been further estimated. Figure 4c shows the temporal evolution of n_p/n_0 , which is quantified following the algorithm described above. In the linear growth stage, n_p/n_0 increases significantly from 0.003% to 0.14%. After the wave saturation at $\sim 328\Omega_e^{-1}$, n_p/n_0 only increases slightly, with a maximum value of $\sim 0.20\%$.

The energy transfer $\overline{\mathbf{E}} \cdot \overline{\mathbf{J}}$ around $0.5\Omega_e$ has been further calculated. Here the fluctuating electric fields $\overline{\mathbf{E}}$ of the wave modes with $\theta = 0^\circ$ ($\theta = 15^\circ$) have been extracted by the band-pass filter in the wave number ranges of $k_x \lambda_e = 0.9\text{--}1.1$ and $|k_y \lambda_e| = 0.0\text{--}0.1$ ($|k_y \lambda_e| = 0.2\text{--}0.3$). Then the energy transfer is given by

$$\overline{\mathbf{E}} \cdot \overline{\mathbf{J}} = E_{\parallel} J_{\parallel} + E_{\perp} J_{\perp} = \sum_{l=1}^{nx} \sum_{m=1}^{ny} E_x J_x / N + \sum_{l=1}^{nx} \sum_{m=1}^{ny} (E_y J_y + E_z J_z) / N$$

where $E_{\parallel} J_{\parallel}$ and $E_{\perp} J_{\perp}$ denote the energy transfer in the parallel and perpendicular direction, E_i and J_i ($i = x, y, z$) represent the three components of wave electric field and current density, N is the number of warm electrons, and \sum means an integration over all grid cells. The negative (positive) $\overline{\mathbf{E}} \cdot \overline{\mathbf{J}}$ means that the energy is transferred from particles (waves) to waves (particles). Figure 5 shows the time history of (a) $E_{\parallel} J_{\parallel}$ and (b) $E_{\perp} J_{\perp}$, in which the wave modes with $\theta = 0^\circ$ and $\theta = 15^\circ$ are denoted by blue and red lines, respectively. The parallel waves are excited from $\sim 100\Omega_e^{-1}$ with negative $E_{\perp} J_{\perp}$, and the nonparallel waves are subsequently generated. During the entire evolution, $E_{\parallel} J_{\parallel}$ of parallel waves is practically 0, due to the negligible parallel electric fields. While that of nonparallel waves is always positive, implying that the plateau-like components are produced due to the Landau resonance with nonparallel waves. At about $370\Omega_e^{-1}$ (denoted by the red arrow), the $E_{\perp} J_{\perp}$ of nonparallel waves becomes positive and the wave modes start to damp. Then the parallel waves also damp from $\sim 405\Omega_e^{-1}$ (marker by the blue arrow). This is consistent with the spectrum evolution in Figures 2b–2f and Movie S1, in which the power gap firstly appears in the nonparallel waves, then in the strictly parallel waves. By distinguish $E_{\perp} J_{\perp}$ of different resonant conditions, we find that the wave damping is mainly contributed by the cyclotron resonance, which has been discussed in H. Chen et al. (2020, 2021). Note that other WNA have also been examined, while the findings remain the same.

Based on 1-D simulation models, several research have been conducted to study the gap formation (H. Chen et al., 2020, 2021; H. Y. Chen et al., 2017; X. Gao et al., 2017; Hsieh & Omura, 2018; J. Li et al., 2019), in which the waves are artificially fixed as nonparallel propagating. While the waves excited by anisotropic electrons have

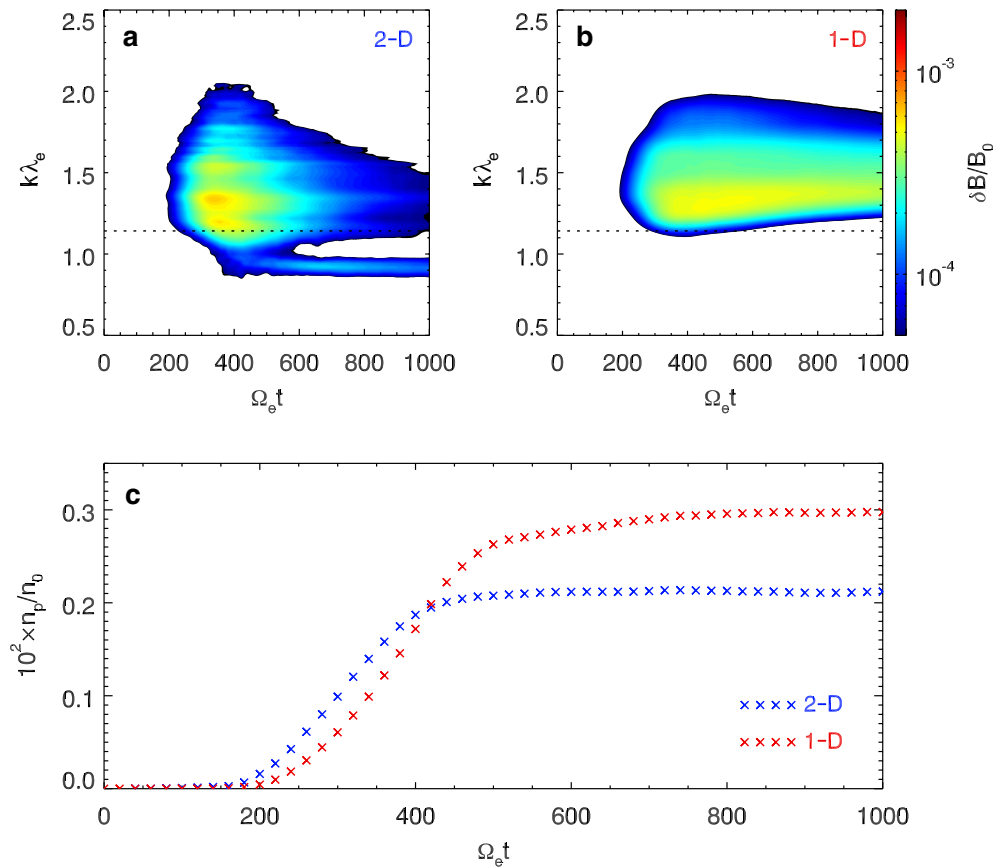


Figure 6. The k - t spectrogram of $\delta B/B_0$ in the (a) 2-D and (b) 1-D models, where the dotted lines represent the wave numbers corresponding to the frequency of $0.5\Omega_e$. (c) The temporal evolutions of n_p/n_0 in the 2-D and 1-D model, which are denoted by the blue and red lines, respectively.

positive growth rates in a wide range of WNAs, and the wave mode with the maximum growth rate propagates along the background magnetic field. Therefore, we have then investigated whether the power gap can be generated by using the same initial setup in both 2-D and 1-D models. A series of cases with different plasma betas ($\beta_{\parallel w} = 0.049$ – 0.360) and temperature anisotropies ($T_{\perp w}/T_{\parallel w} = 3$ – 5) have been performed. In the 1D model, the spatial variation is only allowed in the x direction, and the grid cell is $n_x = 3,072$ with $\Delta x = 0.30\lambda_e$. The background magnetic field is set as $\mathbf{B}_0 = B_0 (\cos\theta\hat{x} + \sin\theta\hat{z})$, where θ is might as well assumed to be $\theta = 20^\circ$. Other parameters keep the same as those in the 2-D models. We have found that when the frequency of the dominant mode ω_d is in the range of 0.4 – $0.6\Omega_e$, the power gap can be generated in both 2-D and 1-D models. However, when ω_d is greater than $0.6\Omega_e$, the power gap can only be formed in the 2-D model. We take the case with $\beta_{\parallel w} = 0.049$ and $T_{\perp w}/T_{\parallel w} = 4$ (with $\omega_d = 0.632\Omega_e$) as an example. Figure 6 illustrates the k - t spectrogram of $\delta B/B_0$ in the (a) 2-D and (b) 1-D models. In the 2-D model, the waves with $\theta = 20^\circ$ have been shown, in which the power gap is formed after the wave frequencies drift to lower values. While the wave frequencies in the 1-D model cannot be lower than $0.5\Omega_e$, and the wave spectrum contains only one band greater than $0.5\Omega_e$. This could be accounted for by the different number densities of plateau-like component (n_p/n_0) in the two models. Figure 6c displays the temporal evolution of n_p/n_0 in the 2-D (blue line) and 1-D (red line) models, which are estimated following the approach in Figure 4a. Although n_p/n_0 in the 1-D model starts to increase later than that in the 2-D model, it can reach up to a greater peak value (0.29% in the 1-D model and 0.21% in the 2-D model), causing more severe damping around $0.5\Omega_e$ (H. Chen et al., 2020, 2021). Therefore, we propose that fixing the WNA as a finite value is unnecessary, as this will artificially enhance the proportion of the plateau-like electron component. The power gap is naturally formed when even a small nonparallel component is excited.

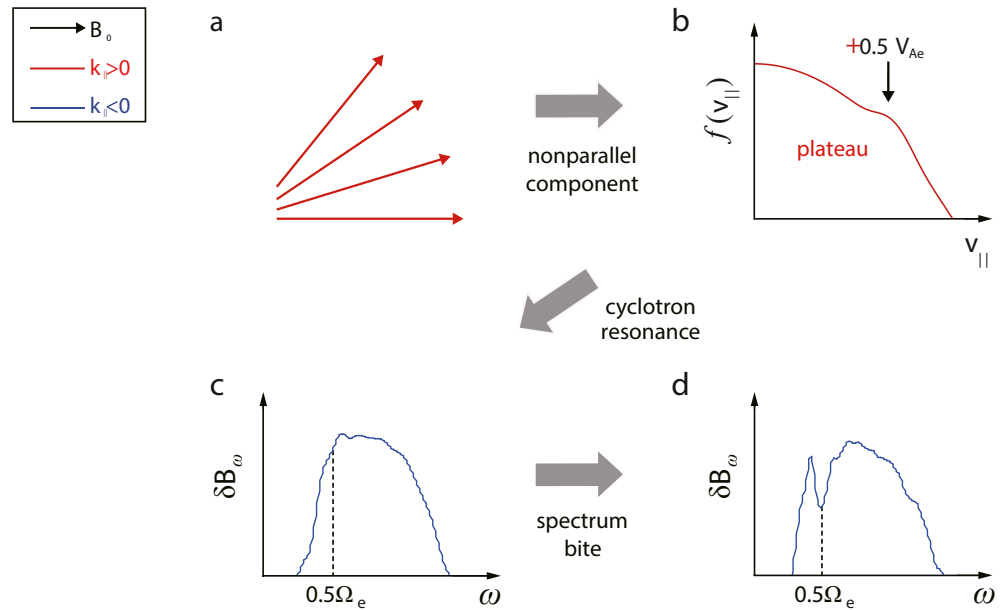


Figure 7. Schematic illustration of the gap formation around $0.5\Omega_e$ due to the damping by the plateau-like electron component in the parallel direction of velocity distribution, named as “spectrum bite”.

4. Summary and Discussion

Using numerical simulations, we have investigated the gap formation around $0.5\Omega_e$ of whistler-mode waves in the Earth’s magnetosphere, which is named as “spectrum bite”. The plateau-like electron components at $\pm 0.5V_{Ae}$, which are produced by the nonparallel waves, can heavily damp the waves around $0.5\Omega_e$. Figure 7 schematically illustrates this mechanism, where the wave modes with positive wave numbers $k_{||} > 0$ (negative ones $k_{||} < 0$) are represented the red (blue) lines. Here we firstly take the wave modes with $k_{||} > 0$ for example (Figure 7a). Both parallel and nonparallel waves are excited, since waves have positive growth rates in a wide WNA range. Although nonparallel waves are weaker than parallel ones, they can produce the plateau-like shape around $+0.5V_{Ae}$ in the parallel electron distribution (Figure 7b). Then, via the cyclotron resonance, the plateau-like electron component causes severe damping in the waves with $k_{||} < 0$ around $0.5\Omega_e$, and the gap forms eventually (Figures 7c and 7d). Note that there is another plateau-like shape forming at around $-0.5V_{Ae}$, since the waves are counter-propagating. Therefore, the wave modes with $k_{||} > 0$ also have a gap, due to the damping by the plateau-like component at $-0.5V_{Ae}$.

Satellite observations have illustrated that the whistler waves with banded structures are typically detected near the equator at relatively larger L-shells ($L > 5$, X. Gao et al., 2019; Teng et al., 2019). To investigate the gap formation in the wave source, we perform the 2-D simulations in a homogeneous magnetic field with periodic boundary conditions. The initial parameters (such as magnetic field strength, plasma beta, and plasma number density) are all typical values at $L = 6$. The simulation domain is in the x range of $[-307.2\lambda_e, 307.2\lambda_e]$ (where the electron inertial length λ_e is estimated as 2.98 km at $L = 6$), which corresponds to a latitude range of $[-1.37^\circ, 1.37^\circ]$. While the source region of whistler waves is confined within $\sim 3^\circ$ around the equator (LeDocq et al., 1998; Teng et al., 2018), implying that our simulation domain is smaller than the wave source. The selection of periodic boundary conditions is acceptable here, since the power gap has already been generated ($\Omega_e t \approx 450$) before waves crossing the simulation domain ($\Omega_e t \approx 1,200$, estimated by the ratio between the length of simulation domain in the x direction and wave phase velocity). Therefore, the “spectrum bite” mechanism can account for the gap formation of whistler waves near the equator.

Based on the dispersion relation of whistler-mode waves (Stix, 1962), the Landau resonance velocity is given as $v_L = \frac{\omega}{k_{||}} = \frac{V_{Ae}}{\cos\theta} \sqrt{\frac{\omega}{\Omega_e} \left(\cos\theta - \frac{\omega}{\Omega_e} \right)}$, which is affected by the wave frequency ω/Ω_e and the WNA θ . Figure 8 illustrates v_L/V_{Ae} as a function of ω/Ω_e for the (a) quasi-parallel waves with WNAs of $\theta = 5^\circ\text{--}30^\circ$ and (b) oblique waves with $\theta = 40^\circ\text{--}70^\circ$. For quasi-parallel waves, v_L/V_{Ae} is in the range of 0.45–0.50 when $\omega/\Omega_e \approx 0.25\text{--}0.70$.

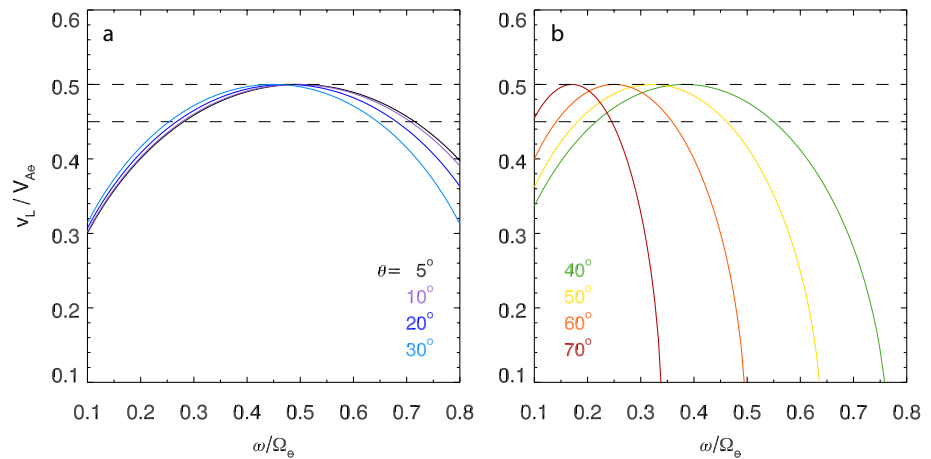


Figure 8. The Landau resonance velocity v_L/V_{Ac} as a function of frequency ω/Ω_e for (a) quasi-parallel waves with $\theta = 5^\circ$ – 30° , and (b) oblique waves with $\theta = 40$ – 70° . The two horizontal lines in each panel represent $v_L = 0.45V_{Ac}$ and $0.50V_{Ac}$.

While for oblique waves, v_L is in a wide range from 0.1 to $0.5V_{Ac}$. In our simulations, whistler waves are excited by anisotropic electrons, and their instabilities mainly concentrate on small angles. Moreover, satellite observations have shown that the waves near the equator are basically quasi-parallel propagating (W. Li et al., 2011; Teng et al., 2018). Therefore, the resonance velocities of these waves are close to $0.5V_{Ac}$ in a wide frequency range. This is also supported by satellite observations, which have shown that the Landau resonant velocities in the parallel electron distribution have always been detected around $0.5V_{Ac}$ in the inner magnetosphere (R. Chen et al., 2019; J. Li et al., 2019; Min et al., 2014). By fixing the waves as nonparallel propagating, H. Chen et al. (2020, 2021) have found that the plateau-like electrons can cause severe damping around $0.5\Omega_e$ through cyclotron resonance, and the power gap is consequently formed. Nevertheless, the wave mode with the largest growth rate is along the background magnetic field (Fan et al., 2019; Gary et al., 2011). It is currently unknown whether this process is still valid in a multi-dimensional frame. By extending to a 2-D PIC model, we have found that even a small proportion of nonparallel wave modes can produce the plateau-like electron component, which can then cause the power gap through spectrum bite. The number density of this component in the simulation is quite low, with a peak value of only $\sim 0.2\%$. In the inner magnetosphere, the proportion of plateau-like electrons associated with whistler waves is typically in the range of 0.01%–1% (R. Chen et al., 2019), providing strong observational support to our study. Furthermore, almost all the wave modes decay after $\sim 500\Omega_e^{-1}$ (Figures 2b–2f and Movie S1), while the waves around $0.5\Omega_e$ are more severely damped among them (Figure 4b), leading to the gap formation. This quite differs from the mechanism in Li et al. (2019), which has proposed that the upper band and lower band waves are excited by two distinct electron populations, while the waves around $0.5\Omega_e$ are unable to grow due to the insufficient anisotropy at $\sim 0.5V_{Ac}$.

Based on a theoretical analysis, Sauer et al. (2020) have indicated that the plateau electrons can cause the damping around $0.5\Omega_e$ in whistler-mode waves. Nevertheless, they haven't talked about how the plateau electrons are produced and how the energy is transferred around $0.5\Omega_e$ are still unknown. By performing 2-D PIC simulations, Ratcliffe and Watt (2017) have also indicated that the plateau distribution can lead to the gap formation. They have initialized the simulations with two anisotropic electron components (warm and hot electrons) to excite whistler-mode waves, and suggested the plateau distribution is modulated through the Landau resonance by the most unstable mode at $\sim 0.5\Omega_e$. In our study, we have explicitly shown that the plateau-like electron component can cause severe damping around $0.5\Omega_e$ through the cyclotron resonance. The plateau-like shape is produced even when there is a small proportion of non-parallel wave modes generated. Moreover, the waves in a large frequency range (not just the wave mode at $\sim 0.5\Omega_e$) can contribute to the formation of plateau-like shape, since their Landau resonance velocities are all close to $0.5V_{Ac}$. Last but not the least, the constraint on initial setup in Ratcliffe and Watt (2017) can be further relaxed by using only one anisotropic electron population. Our study provides an important clue that the plateau electron component may be the key to solving this long-standing mystery.

During the propagation from the source region toward higher latitudes, the whistler-mode waves have frequency chirping due to the inhomogeneous field, leading to the generation of chorus waves (Katoh & Omura, 2006, 2007; Ke et al., 2020; Lu et al., 2019). Since our simulations are performed in a homogeneous environment, the “spectrum bite” mechanism is only limited to broad-band whistler-mode waves. To study both the generation of chorus waves and the formation of power gap in a full particle simulation is necessary but requires huge computation resources, which is beyond the scope of this paper and left to further study.

Data Availability Statement

The simulation data are archived in <https://dx.doi.org/10.12176/01.99.00471>.

Acknowledgments

This work was supported by the Strategic Priority Research Program of Chinese Academy of Sciences Grant Nos. XDB41000000, Key Research Program of Frontier Sciences CAS (QYZDJ-SSW-DQC010), USTC Research Funds of the Double First-Class Initiative (YD3420002001), the Fundamental Research Funds for the Central Universities (WK3420000013), and “USTC Tang Scholar” program. The authors acknowledge for the data resource from National Space Science Data Center, National Science & Technology Infrastructure of China (<http://www.nssdc.ac.cn>).

References

- Burtis, W. J., & Helliwell, R. A. (1969). Banded chorus a new type of VLF radiation observed in the magnetosphere by OGO 1 and OGO 3. *Journal of Geophysical Research*, 74(11), 3002–3010. <https://doi.org/10.1029/JA074i011p03002>
- Chen, H., Gao, X., Lu, Q., Sauer, K., Chen, R., Yao, J., & Wang, S. (2021). Gap formation around 0.5Ω_{ce} of whistler-mode waves excited by electron temperature anisotropy. *Journal of Geophysical Research: Space Physics*, 126(2), e2020JA028631. <https://doi.org/10.1029/2020JA028631>
- Chen, H., Lu, Q., Wang, X., Fan, K., Chen, R., & Gao, X. (2022). One-dimensional gcPIC-δf simulation of hooked chorus waves in the Earth's inner magnetosphere. *Geophysical Research Letters*, 49(4), e2022GL097989. <https://doi.org/10.1029/2022GL097989>
- Chen, H., Sauer, K., Lu, Q., Gao, X., & Wang, S. (2020). Two-band whistler-mode waves excited by an electron bi-Maxwellian distribution plus parallel beams. *AIP Advances*, 10(12), 125010. <https://doi.org/10.1063/5.0026220>
- Chen, H. Y., Gao, X. L., Lu, Q. M., Ke, Y. G., & Wang, S. (2017). Lower band cascade of whistler waves excited by anisotropic hot electrons: One dimensional PIC simulations. *Journal of Geophysical Research: Space Physics*, 122(10), 10448–10457. <https://doi.org/10.1002/2017JA024513>
- Chen, L. J., Thorne, R. M., Li, W., & Bortnik, J. (2013). Modeling the wave normal distribution of chorus waves. *Journal of Geophysical Research*, 118(3), 1074–1088. <https://doi.org/10.1029/2012JA018343>
- Chen, R., Gao, X., Lu, Q., & Wang, S. (2019). Unraveling the correlation between chorus wave and electron beam-like distribution in the Earth's magnetosphere. *Geophysical Research Letters*, 46(21), 11671–11678. <https://doi.org/10.1029/2019GL085108>
- Fan, K., Gao, X., Lu, Q., Guo, J., & Wang, S. (2019). The effects of thermal electrons on whistler mode waves excited by anisotropic hot electrons: Linear theory and 2-D PIC simulations. *Journal of Geophysical Research: Space Physics*, 124(7), 5234–5245. <https://doi.org/10.1029/2019JA026463>
- Fu, X., Cowee, M. M., Friedel, R. H., Funsten, H. O., Gary, S. P., Hospodarsky, G. B., et al. (2014). Whistler anisotropy instabilities as the source of banded chorus: Van Allen Probes observations and particle-in-cell simulations. *Journal of Geophysical Research: Space Physics*, 119(10), 8288–8298. <https://doi.org/10.1002/2014JA020364>
- Fu, X., Gary, S. P., Reeves, G. D., Winske, D., & Woodroffe, J. R. (2017). Generation of highly oblique lower band chorus via nonlinear three-wave resonance. *Geophysical Research Letters*, 44(19), 9532–9538. <https://doi.org/10.1002/2017GL074411>
- Gao, X., Chen, L., Li, W., Lu, Q., & Wang, S. (2019). Statistical results of the power gap between lower-band and upper-band chorus waves. *Geophysical Research Letters*, 46(8), 4098–4105. <https://doi.org/10.1029/2019GL082140>
- Gao, X., Ke, Y., Lu, Q., Chen, L., & Wang, S. (2017). Generation of multiband chorus in the Earth's magnetosphere: 1-D PIC simulation. *Geophysical Research Letters*, 44(2), 618–624. <https://doi.org/10.1002/2016GL072251>
- Gao, X., Lu, Q., & Wang, S. (2018). Statistical results of multiband chorus by using THEMIS waveform data. *Journal of Geophysical Research: Space Physics*, 123(7), 5506–5515. <https://doi.org/10.1029/2018JA025393>
- Gao, X. L., Li, W., Thorne, R. M., Bortnik, J., Angelopoulos, V., Lu, Q. M., et al. (2014). New evidence for generation mechanisms of discrete and hiss-like whistler mode waves. *Geophysical Research Letters*, 41(14), 4805–4811. <https://doi.org/10.1002/2014gl060707>
- Gao, X. L., Lu, Q. M., Bortnik, J., Li, W., Chen, L. J., & Wang, S. (2016). Generation of multiband chorus by lower band cascade in the Earth's magnetosphere. *Geophysical Research Letters*, 43(6), 2343–2350. <https://doi.org/10.1002/2016GL068313>
- Gary, S. P., Liu, K., & Winske, D. (2011). Whistler anisotropy instability at low electron: Particle-in-cell simulations. *Physics of Plasmas*, 18(8), 082902. <https://doi.org/10.1063/1.3610378>
- Hikishima, M., Omura, Y., & Summers, D. (2010). Microburst precipitation of energetic electrons associated with chorus wave generation. *Geophysical Research Letters*, 37(7), L07103. <https://doi.org/10.1029/2010GL042678>
- Horne, R. B., Thorne, R. M., Meredith, N. P., & Anderson, R. R. (2003). Diffuse auroral electron scattering by electron cyclotron harmonic and whistler mode waves during an isolated substorm. *Journal of Geophysical Research*, 108(A7), 1290. <https://doi.org/10.1029/2002JA009736>
- Hsieh, Y.-K., & Omura, Y. (2018). Nonlinear damping of oblique whistler mode waves via Landau resonance. *Journal of Geophysical Research: Space Physics*, 123(9), 7462–7472. <https://doi.org/10.1029/2018JA025848>
- Kasahara, S., Miyoshi, Y., Yokota, S., Mitani, T., Kasahara, Y., Matsuda, S., et al. (2018). Pulsating aurora from electron scattering by chorus waves. *Nature*, 554(7692), 337–340. <https://doi.org/10.1038/nature25505>
- Katoh, Y., & Omura, Y. (2006). A study of generation mechanism of VLF triggered emission by self-consistent particle code. *Journal of Geophysical Research*, 111(A12), A12207. <https://doi.org/10.1029/2006JA011704>
- Katoh, Y., & Omura, Y. (2007). Computer simulation of chorus wave generation in the Earth's inner magnetosphere. *Geophysical Research Letters*, 34(3), L03102. <https://doi.org/10.1029/2006GL028594>
- Ke, Y., Gao, X., Lu, Q., Wang, X., & Wang, S. (2017). Generation of rising tone chorus in a two-dimensional mirror field by using the general curvilinear PIC code. *Journal of Geophysical Research: Space Physics*, 122(8), 8154–8165. <https://doi.org/10.1002/2017JA024178>
- Ke, Y., Lu, Q., Gao, X., Wang, X., Chen, L., Wang, S., & Wang, S. (2020). Particle-in-cell simulations of characteristics of rising-tone chorus waves in the inner magnetosphere. *Journal of Geophysical Research: Space Physics*, 125(7), e2020JA027961. <https://doi.org/10.1029/2020JA027961>
- LeDocq, M. J., Gurnett, D. A., & Hospodarsky, G. B. (1998). Chorus source locations from VLF Poynting flux measurements with the Polar spacecraft. *Geophysical Research Letters*, 25(21), 4063–4066. <https://doi.org/10.1029/1998GL900071>
- Li, J., Bortnik, J., An, X., Li, W., Angelopoulos, V., Thorne, R. M., et al. (2019). Origin of two-band chorus in the radiation belt of Earth. *Nature Communications*, 10(1), 4672. <https://doi.org/10.1038/s41467-019-12561-3>

- Li, W., Bortnik, J., Thorne, R. M., & Angelopoulos, V. (2011). Global distribution of wave amplitudes and wave normal angles of chorus waves using THEMIS wave observations. *Journal of Geophysical Research*, *116*(A12), A12205. <https://doi.org/10.1029/2011JA017035>
- Liu, K., Gary, S. P., & Winske, D. (2011). Excitation of banded whistler waves in the magnetosphere. *Geophysical Research Letters*, *38*(14), L14108. <https://doi.org/10.1029/2011GL048375>
- Lu, Q., Chen, L., Wang, X., Gao, X., Lin, Y., & Wang, S. (2021). Repetitive emissions of rising-tone chorus waves in the inner magnetosphere. *Geophysical Research Letters*, *48*(15), e2021GL094979. <https://doi.org/10.1029/2021GL094979>
- Lu, Q., Ke, Y., Wang, X., Liu, K., Gao, X., Chen, L., & Wang, S. (2019). Two-dimensional general curvilinear particle-in-cell (gcPIC) simulation of rising-tone chorus waves in a dipole magnetic field. *Journal of Geophysical Research: Space Physics*, *124*(6), 4157–4167. <https://doi.org/10.1029/2019ja026586>
- Min, K., Liu, K., & Li, W. (2014). Signatures of electron Landau resonant interactions with chorus waves from THEMIS observations. *Journal of Geophysical Research: Space Physics*, *119*(7), 5551–5560. <https://doi.org/10.1002/2014JA019903>
- Ni, B., Thorne, R. M., Shprits, Y. Y., & Bortnik, J. (2008). Resonant scattering of plasma sheet electrons by whistler-mode chorus: Contribution to diffuse auroral precipitation. *Geophysical Research Letters*, *35*(11), L11106. <https://doi.org/10.1029/2008GL034032>
- Omura, Y., Hikishima, M., Katoh, Y., Summers, D., & Yagitani, S. (2009). Nonlinear mechanisms of lower-band and upper-band VLF chorus emissions in the magnetosphere. *Journal of Geophysical Research*, *114*(A7), A07217. <https://doi.org/10.1029/2009JA014206>
- Ratcliffe, H., & Watt, C. E. J. (2017). Self-consistent formation of a 0.5 cyclotron frequency gap in magnetospheric whistler mode waves. *Journal of Geophysical Research: Space Physics*, *122*(8), 8166–8180. <https://doi.org/10.1002/2017JA024399>
- Santolík, O., Gurnett, D. A., Pickett, J. S., Parrot, M., & Cornilleau-Wehirlin, N. (2005). Central position of the source region of storm-time chorus. *Planetary and Space Science*, *53*(1–3), 299–305. <https://doi.org/10.1016/j.pss.2004.09.056>
- Sauer, K., Baumgärtel, K., & Sydora, R. (2020). Gap formation around $\Omega_e/2$ and generation of low-band whistler waves by Landau-resonant electrons in the magnetosphere: Predictions from dispersion theory. *Earth and Planetary Physics*, *4*(2), 1–13. <https://doi.org/10.26464/epp2020020>
- Stix, T. H. (1962). *The theory of plasma waves*. McGraw-Hill.
- Summers, D., Thorne, R. M., & Xiao, F. (1998). Relativistic theory of wave-particle resonant diffusion with application to electron acceleration in the magnetosphere. *Journal of Geophysical Research*, *103*(A9), 20487–20500. <https://doi.org/10.1029/98JA01740>
- Teng, S., Tao, X., & Li, W. (2019). Typical characteristics of whistler mode waves categorized by their spectral properties using Van Allen Probes observations. *Geophysical Research Letters*, *46*(7), 3607–3614. <https://doi.org/10.1029/2019GL082161>
- Teng, S., Tao, X., Li, W., Qi, Y., Gao, X., Dai, L., et al. (2018). A statistical study of the spatial distribution and source-region size of chorus waves using Van Allen Probes data. *Annales de Geophysique*, *36*(3), 867–878. <https://doi.org/10.5194/angeo-36-867-2018>
- Thorne, R. M., Li, W., Ni, B., Ma, Q., Bortnik, J., Chen, L., et al. (2013). Rapid local acceleration of relativistic radiation-belt electrons by magnetospheric chorus. *Nature*, *504*(7480), 411–414. <https://doi.org/10.1038/nature12889>
- Tsurutani, B. T., Lakhina, G. S., & Verkhoglyadova, O. P. (2013). Energetic electron (>10 keV) microburst precipitation, 5–15 s X-ray pulsations, chorus, and wave-particle interactions: A review. *Journal of Geophysical Research: Space Physics*, *118*(5), 2296–2312. <https://doi.org/10.1002/jgra.50264>
- Tsurutani, B. T., & Smith, E. J. (1974). Postmidnight chorus: A substorm phenomenon. *Journal of Geophysical Research*, *79*(1), 118–127. <https://doi.org/10.1029/JA079i001p00118>
- Tsurutani, B. T., & Smith, E. J. (1977). Two types of magnetospheric ELF chorus and their substorm dependences. *Journal of Geophysical Research*, *82*(32), 5112–5128. <https://doi.org/10.1029/JA082i032p05112>
- Xie, H., & Xiao, Y. (2016). PDRK: A general kinetic dispersion relation solver for magnetized plasma. *Plasma Science and Technology*, *18*(2), 97–107. <https://doi.org/10.1088/1009-0630/18/2/01>